ELSEVIER

International Journal of Solids and Structures 41 (2004) 305–322

INTERNATIONAL JOURNAL OF SOLIDS and STRUCTURES

www.elsevier.com/locate/ijsolstr

Pertinence of the grains aggregate type on the self-consistent model responses

A. Abdul-Latif *

L3M, IUT de Tremblay, GIM, Rue de la Raperie, 93290 Tremblay-en-France, France

Received 9 September 2003; received in revised form 9 September 2003

Abstract

The effect of the aggregate of grains type (i.e., the number and the orientation of grains) on the non-linear strain–stress behavior of FCC polycrystals is of particular interest in the present work. In this context, a well established self-consistent model, proposed by the author and co-workers [J. Appl. Mech. 69 (2002) 309] is used. This model is tested under different complex cyclic loading paths with strain and stress-controlled conditions describing especially the multiaxial ratcheting behavior of stainless steel 316L which represents also another main goal of this work. In order to study the aggregate effect on the overall and local responses of polycrystals, several initially random crystal distributions are tested under these loading situations. It is recognized that the model shows a noticeable sensitivity to the aggregate type principally under stress-controlled cyclic loading paths. Accordingly, it can be considered that the aggregate of grains represents a model parameter needing identification. Moreover, the connection between the aggregate constitution and the form of the loading paths play also an important role on the predicted responses of polycrystals.
© 2003 Elsevier Ltd. All rights reserved.

Keywords: Self-consistent model; Aggregate influence; Multiaxial ratcheting; Local heterogeneity

1. Introduction

The mechanical responses of single or poly-phase polycrystals are typical examples of heterogeneous behavior of such material at their local geometry. In term of the irreversible behavior, their inelastic flow is a manifestation of their heterogeneity and their discrete and heterogeneous deformation pattern at the microscale. This leads, in general, to strengthening and workhardening of polycrystals. At the granular level, the heterogeneity comes widely form the differences in the orientation of the grains and the single-crystal anisotropy since the morphology and spatial distribution of the grains are not taken into account. Crystals are consequently heterogeneous and some crystals deform differently than others inducing highly non-uniform strain fields. Hence, the knowledge of the local heterogeneities is considerably important in modeling of the overall stress–strain behavior of polycrystals. The exact solution for the local fields in these

* Tel.: +33-1-41-51-12-34; fax: +33-1-41-51-12-49/48-61-38-17.
E-mail address: aabdul@iu2t.univ-paris8.fr (A. Abdul-Latif).

0020-7683/$ - see front matter © 2003 Elsevier Ltd. All rights reserved.
doi:10.1016/j.ijsolstr.2003.09.014

crystals even under homogenous overall boundary conditions is a extremely difficult task. However, exact solutions for local stress and strains exist in many cases (Dvorak and Benveniste, 1996). The polycrystal is usually considered as an aggregate of numerous grains with different orientations with respect to the loading axis. The single-phase material properties of each grain are identical with respect to the crystallographic reference system.

In the framework of the self-consistent approach initially proposed by Kröner (1961) and by Budiansky and Wu (1962), a large number of solutions has been obtained for different problems. Even having so restricted scope, it is impossible to cover all investigations of the problem and make complete list of references. Therefore, only the main articles related directly to the present work will be mentioned. Such approaches consider the problem of an inclusion (grain) embedded in and interacting with a homogenous equivalent medium (HEM: being an average neighborhood of all these grains) namely the matrix. Neglected the topology of the aggregate, they fulfill the compatibility and stress equilibrium in an average sense (consistency conditions). The local response is generally non-linear leading approximately to an overall non-linear response. This permits a calculation of the unknown overall moduli that describe the HEM response. Furthermore, the heterogeneity at the granular level represents the main factor related to localized intergranular interactions. Up to now, this can not be realistically described by most of the self-consistent approaches. As for the relative anisotropy of the grain and matrix, such approaches give a better description of material response than classical upper-bound models. In the current investigation, an attention will be concentrated on those solutions dealing with the polycrystals cyclic behavior problem under different loading paths.

Once the number of grains plays an important role on the predicted result accuracy, hence the emphasize is placed here on the single-phase FCC polycrystals of random distribution. It is noteworthy that many cyclic phenomena such as Bauschinger effect, strain memory effect and additional hardening have been faithfully described by the model under different loading conditions (Dingli et al., 2000). The effect of the grains aggregate type on the overall responses has been investigated under cyclic strain-controlled situations (e.g., Cailletaud, 1987; Pilvin, 1990; Abdul-Latif et al., 1998), under low cycle fatigue (Abdul-Latif and Saanouni, 1997) and under high cycle fatigue (Bennett and McDowell, 2003). In fact, they concluded that the used model is almost not sensitive to the aggregate type under these loading paths. However, this parameter, as we think, is not yet studied under stress-controlled conditions. Therefore, its effect on the predicted responses (overall and local) of polycrystals, representing the principal purpose of this work, is carefully studied. Moreover, an attention is made on the cyclic stress-controlled loading to describe one of the most complicated material behavior. It is a matter of the multiaxial ratcheting behavior of polycrystals. Several numerical simulations are conducted to reproduce the mechanical behavior of stainless steel 316L. Thus, six initially random crystal distributions (40, 200, 300, 400, 504 and 2016 grains) are tested to elucidate the model sensitivity to this factor. Comparisons between predictions and experimental results are also performed under these loading conditions.

2. The used self-consistent model

The main purpose of the self-consistent polycrystal approaches is to deduce the overall response of the aggregate from the known properties of the grains and the interaction relation of each grain with its environment. The type of the interaction (hard or soft) of the grain with its matrix gives an appropriate estimation about the accommodated plastic strain and its repartition between the grain and the surrounding. We limit ourselves to a short description of the main features of the used model. For further discussion about this model the reader is referred to the reference (Abdul-Latif et al., 2002). With the small strain assumption, the model uses three different levels, namely macroscopic (representative volume element—RVE: aggregate of grains), granular and microscopic (crystallographic slip system—css). It is im-

portant to keep in mind that the RVE represents here a material point from a modeling point of view. As a starting point, it is assumed that slip is the dominant deformation mechanism and other mechanisms like twinning, grain boundary sliding, etc, are neglected. For the single crystal modeling, the resolved shear stress (τ^s) is obtained on each slip system at a grain by twice-contracted tensorial product between the granular stress $\underline{\sigma}^g$ and the Schmid factor matrix (orientation tensor) $\underline{m}^s$.

$$\tau^s = \underline{\sigma}^g : \underline{m}^s, \tag{1}$$

$$\underline{m}^s = \tfrac{1}{2}[\mathbf{n}^s \otimes \mathbf{b}^s + \mathbf{n}^s \otimes \mathbf{b}^s], \tag{2}$$

where $\mathbf{b}^s$ is the unit vector in the slip direction and $\mathbf{n}^s$ being the vector normal to the slip plane.

At the css level, only one couple of intragranular isotropic hardening variables (q^s, R^s) is introduced describing the expansion of the elastic domain of the system s:

$$R^s = Q^s \sum_{r=1}^{n} H_{rs} q^r, \tag{3}$$

$$\dot{q}^s = \dot{\lambda}^s (1 - b^s q^s). \tag{4}$$

This hardening is defined by its modulus Q^s and its non-linearity coefficient b^s. H_{rs} is the hardening interaction matrix allowing the introduction of the cross influence of the slip of the system 's' on the hardening of the system 'r', belonging to the same family or not. Only the octahedral slips $\{1\,1\,1\}\langle 1\,1\,0\rangle$ for FCC materials are taken into account. Hence, a simple 12×12 matrix is chosen. At this level, the local inelastic flow is determined by adopting a threshold concept, i.e., a slip system is plastified when the absolute value of its resolved shear stress τ^s is greater than the actual flow surface radius $(R^s + k_0^s)$. The slip rate can be determined as long as the shear stress and the hardening variables are known. Thus, the yield surface (f^s) for each slip system is expressed by

$$f^s = |\tau^s| - R^s - k_0^s, \tag{5}$$

where k_0^s is the initial value of the critical resolved shear stress.

In the framework of viscoplasticity, the value of pseudo-multiplier $\dot{\lambda}^s$ (accumulated slip rate), for each slip system, is a power function of the distance to the yield point defined by the criterion f^s:

$$\dot{\lambda}^s = \left(\frac{f^s}{K^s}\right)^{z^s} = \left(\frac{|\tau^s| - R^s - k_0^s}{K^s}\right)^{z^s}, \tag{6}$$

K^s and z^s are two parameters characterizing the viscous sensitivity of the material.

It is assumed that the slip is the dominant deformation mechanism, the granular inelastic strain rate ($\dot{\underline{\varepsilon}}^g_{in}$) is therefore deduced as the sum of the contribution from all activated slip systems:

$$\dot{\underline{\varepsilon}}^g_{in} = \sum_{s=1}^{n} \dot{\lambda}^s \operatorname{sign}(\tau^s) \underline{m}^s = \sum_{s=1}^{n} \dot{\gamma}^s \underline{m}^s \tag{7}$$

with

$$\dot{\gamma}^s = \dot{\lambda}^s \operatorname{sign}(\tau^s), \tag{8}$$

where $\dot{\gamma}^s$ is the slip rate on the css.

From a physical viewpoint, the granular elastic behavior is generally anisotropic. The principal objective of the micromechanical model is to describe the cyclic plasticity of polycrystals. For the sake of theoretical simplicity, the granular elastic behavior is assumed to be uniform, isotropic and compressible. Moreover, the corresponding constitutive equations including their accompanying parameters are the

same in each grain. However, it is important to note that the heterogeneity of the elastic behavior within the RVE depends principally upon the local geometrical position of each grain with respect to the loading axis since the size, the morphology and spatial distribution of the grains are not taken into account. Consequently, the elastic strain $\underline{\varepsilon}_{\mathrm{e}}^{g}$ is defined by a well-known isotropic elastic equation at the granular level:

$$\underline{\sigma}^{g} = 2\mu\underline{\varepsilon}_{\mathrm{e}}^{g} + \lambda(\mathrm{tr}\underline{\varepsilon}_{\mathrm{e}}^{g})\underline{I}, \tag{9}$$

where $\underline{I}$ is the second order unit tensor. In the isothermal case, the granular Lame's coefficients (λ and μ) remain always constant, hence the time derivative of Eq. (9) gives

$$\dot{\underline{\varepsilon}}_{\mathrm{e}}^{g} = \frac{\dot{\underline{\sigma}}^{g}}{2\mu} - \frac{\lambda}{2\mu(2\mu+3\lambda)}\mathrm{tr}(\dot{\underline{\sigma}}^{g})\underline{I}. \tag{10}$$

According to the small strain hypothesis, the total granular strain $\underline{\varepsilon}^{g}$ is partitioned into elastic $\underline{\varepsilon}_{\mathrm{e}}^{g}$ and inelastic $\underline{\varepsilon}_{\mathrm{in}}^{g}$ parts:

$$\underline{\varepsilon}^{g} = \underline{\varepsilon}_{\mathrm{e}}^{g} + \underline{\varepsilon}_{\mathrm{in}}^{g}. \tag{11}$$

The index $s \in \{1, 2, 3, \ldots, n\}$ is associated with the slip system rank with (n) being the maximum number of octahedral systems in the grain ($n = 12$ for FCC microstructures). Similarly, the index $g \in \{1, 2, 3, \ldots, N_{\mathrm{g}}\}$ describes the grain rank with N_{g} being the maximum number of grains contained in the aggregate.

Since the overall behavior of polycrystals is strongly influenced by grain/matrix interaction law, therefore the heterogeneous stress and strain fields throughout the matrix (aggregate) need grain interaction consideration. A trivial way to theoretically obtain this interaction is the well-known self-consistent relations. Thus, the interaction law represents an extremely important key factor for this type of modeling.

A succinct theoretical presentation is given here summarizing the basic assumptions which have been adopted by Abdul-Latif et al. (2002) in order to derive the interaction law.

The generalized elastic–viscoplastic interaction law of Molinari et al. (1997) is expressed as follows:

$$\left(\underline{\underline{\mathfrak{I}}}^{s^{-1}} + \underline{\underline{C}}\right)^{-1} : (\dot{\underline{\sigma}}^{g} - \dot{\underline{\Sigma}}) + \left(\underline{\underline{\mathfrak{I}}}'^{s^{-1}} + \underline{\underline{A}}\right)^{-1} : (\underline{s}^{g} - \underline{S}) = (\dot{\underline{\varepsilon}}^{g} - \dot{\underline{E}}). \tag{12}$$

$\underline{\underline{\mathfrak{I}}}^{s}$ and $\underline{\underline{\mathfrak{I}}}'^{s}$ are respectively fourth rank tensors which have to be computed using $\underline{\underline{A}}$ and $\underline{\underline{C}}$ with Green function and integral methods, respectively. Where, $\underline{\underline{C}}$ is the global stiffness tensor. The fourth order tensor $\underline{\underline{A}}$ represents the macroscopic tangent modulus. $\dot{\underline{\varepsilon}}^{g}$ and $\dot{\underline{E}}$ are respectively the total granular and overall strain rates.

In the case where the elastic response dominates, the viscoplastic term $\left(\underline{\underline{\mathfrak{I}}}'^{s^{-1}} + \underline{\underline{A}}\right)^{-1}$ becomes negligible with respect of the elastic part, and the interaction law can be written by

$$\left(\underline{\underline{\mathfrak{I}}}^{s^{-1}} + \underline{\underline{C}}\right)^{-1} : (\dot{\underline{\sigma}}^{g} - \dot{\underline{\Sigma}}) = (\dot{\underline{\varepsilon}}_{\mathrm{e}}^{g} - \dot{\underline{E}}_{\mathrm{e}}). \tag{13}$$

It corresponds to the solution of the elasticity problem for heterogeneous materials. For a spherical inclusion embedded in a finite homogenous isotropic matrix having elastic properties defined by μ and λ, the fourth order interaction tensor is determined by François et al. (1993). Therefore, the elastic part of the interaction law can be expressed by

$$2A(\dot{\underline{\sigma}}^{g} - \dot{\underline{\Sigma}}) + B\mathrm{tr}(\dot{\underline{\sigma}}^{g} - \dot{\underline{\Sigma}})\underline{1} = (\dot{\underline{\varepsilon}}_{\mathrm{e}}^{g} - \dot{\underline{E}}_{\mathrm{e}}), \tag{14}$$

where the constants A and B are defined as

$$A = \frac{-(8\mu + 3\lambda)}{2\mu(14\mu + 9\lambda)}, \tag{15}$$

$$B = \frac{(6\mu + \lambda)(3\lambda + 8\mu)}{\mu(448\mu^2 + 456\mu\lambda + 108\lambda^2)}. \tag{16}$$

For a fully viscoplastic behavior dominating at stationary state (in the long range response), the term $(\dot{\underline{\sigma}}^g - \dot{\underline{\Sigma}})$ is practically vanished. Therefore, Eq. (12) can be written approximately as

$$\left(\underline{\underline{\mathfrak{I}}}^{ts^{-1}} + \underline{\underline{A}}\right)^{-1} : (\underline{s}^g - \underline{S}) = (\dot{\underline{\varepsilon}}^g_{\text{in}} - \dot{\underline{E}}_{\text{in}}). \tag{17}$$

This equation represents a self-consistent approach developed by Molinari et al. (1987) describing the viscoplastic behavior of polycrystals under large deformation condition. In the case where the viscoplastic behavior of the matrix is supposed isotropic and incompressible for spherical inclusion, the viscoplastic part of the general interaction law (12) is thus deduced as

$$-\frac{1}{3\eta^0}(\underline{s}^g - \underline{S}) = (\dot{\underline{\varepsilon}}^g_{\text{in}} - \dot{\underline{E}}_{\text{in}}). \tag{18}$$

The general interaction law for the elastic–viscoplastic behavior of polycrystal (Eq. (12)) is equal to the sum of the two approximate parts (elastic: Eq. (14) and viscoplastic: Eq. (18)). Thus, one obtains

$$2A(\dot{\underline{\sigma}}^g - \dot{\underline{\Sigma}}) + B\text{tr}(\dot{\underline{\sigma}}^g - \dot{\underline{\Sigma}})\underline{1} - \frac{1}{3\eta^0}(\underline{s}^g - \underline{S}) = (\dot{\underline{\varepsilon}}^g - \dot{\underline{E}}). \tag{19}$$

The same problem of η^0 adjustment, as in the incompressible case (Abdul-Latif et al., 1998), is came across in order to satisfy the self-consistency conditions especially under multiaxial loading paths. According to Abdul-Latif et al. (2002), the term $(1/3\eta^0)$ is thus replaced by a phenomenological parameter $(\alpha > 0)$ and the simplified interaction law is written as

$$2A(\dot{\underline{\sigma}}^g - \dot{\underline{\Sigma}}) + B\text{tr}(\dot{\underline{\sigma}}^g - \dot{\underline{\Sigma}})\underline{1} - \alpha(\underline{s}^g - \underline{S}) = (\dot{\underline{\varepsilon}}^g - \dot{\underline{E}}). \tag{20}$$

The overall properties are determined by the collective properties of the constituents (crystals). Since the size, morphology, spatial distribution of the grains and the neighboring effect are not taken into consideration by the model, therefore the transition from the single to the polycrystal response is performed by classical averaging procedures depending on the granular rates. In this context, the overall elastic and inelastic strain tensors are obtained through the micro–macro methodology. Thus, the overall elastic strain rate $(\dot{\underline{E}}^{\text{e}})$ is calculated by

$$\dot{\underline{E}}^{\text{e}} = \sum_{g=1}^{N_{\text{g}}} v^g \dot{\underline{\varepsilon}}^g_{\text{e}}. \tag{21}$$

The overall inelastic strain rate $(\dot{\underline{E}}^{\text{in}})$ is deduced by the following equation:

$$\dot{\underline{E}}^{\text{in}} = \sum_{g=1}^{N_{\text{g}}} v^g \dot{\underline{\varepsilon}}^g_{\text{in}}, \tag{22}$$

where v^g is the volume fraction of the same oriented grains. $\dot{\underline{\varepsilon}}^g_{\text{e}}$ and $\dot{\underline{\varepsilon}}^g_{\text{in}}$ are determined by Eqs. (10) and (7), respectively.

The overall total strain rate $(\dot{\underline{E}})$ is determined as follows:

$$\dot{\underline{E}} = \dot{\underline{E}}^{\text{e}} + \dot{\underline{E}}^{\text{in}}. \tag{23}$$

As far as the hardening behavior is concerned, two sources of kinematic hardening are physically observed at two levels: the first one (intergranular) comes from the plastic strain incompatibility between grains giving non-uniform distribution of the stresses at granular level. The second source (intragranular) represents the long-range interactions inside the grain. In fact, the effects of these hardening types can be naturally described by the interaction law without proposing internal variables under uniaxial and multiaxial cyclic paths. This is due to the existence of the granular elastic behavior in the interaction law since the intergranular accommodation has an elastic nature. It is worth intriguing that the kinematic hardening effect depends considerably on the scalar parameter α (Eq. (20)), which is independent on the strain history and is capable to satisfy the self-consistency condition at each instant. The influence of this parameter on the polycrystals hardening (kinematic and isotropic) is studied using the yield surface evolution concept. Hence, two different values of α (5×10^{-7} and 5×10^{-6}) are chosen for describing the initial and subsequent yield surfaces employing the 200-grain aggregate as an example. Plotted in a stress-space, numerical constructions of these surfaces are conducted. The initial yield surface is determined by following radial stress path away from the origin of the stress-space, always returning to the origin after yielding. An offset of 4×10^{-4} s^{-1}, as a macroscopic equivalent inelastic strain rate, is applied. The isotropic hardening effect, which describes the expansion of the elastic domain, is also examined showing its effect on the subsequent yield surface. An examination of Fig. 1 shows that the initial surface is smooth and circular. This result is expected since the assumption of the isotropic elastic behavior is adopted by the model. The subsequent yield surfaces are obtained after prestraining in axial direction ($E_{11} = 0.008$), then, they are constructed after a partial unloading followed by reloading in different directions. These surfaces are expanded, translated and distorted in the prestraining direction. Governing mainly by the overall kinematic hardening effect, the distortion of this surface is characterized by the appearance of a round nose formed in the prestraining direction and a flat in the opposite one. Variation the value of the parameter α shows obviously its effect on the kinematic hardening evolution and consequently on the subsequent yield surface. Moreover, the isotropic hardening evolution is also influenced by α as it has been shown by Dingli et al. (2000).

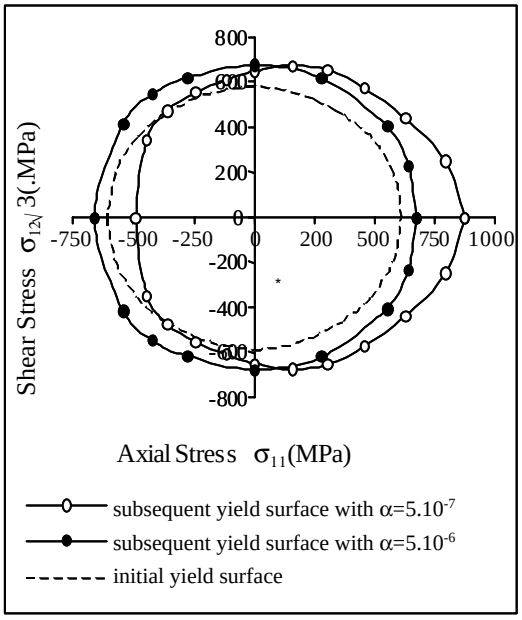

Fig. 1. Effect of the parameter α on the yield surface evolution.

Indeed, this parameter has to be determined in such a manner that the instantaneous elastic effect and the viscoplastic relaxation at steady state are appropriately ensured. If these two conditions are well respected, the overall kinematic and isotropic hardenings will be successfully described (Abdul-Latif et al., 2002). The parameter (α) has also a primordial role on the activated slip systems (Dingli et al., 2000). Actually, the existence of the heterogeneous granular elastic behavior in the interaction law leads to a natural description of the kinematic hardening effect. In the light of this fact, with the value of $\alpha = 5 \times 10^{-7}$, the overall kinematic and isotropic hardening effects on the related subsequent yield surface are noticeable (Fig. 1), i.e., expansion, translating and distortion of this surface are well demonstrated. Concerning the second value of α (5×10^{-6}), an expansion of the elastic domain which is associated with isotropic hardening effects, is well recorded. This due to the fact that a progressive activation of the slip systems is clearly taken place (Dingli et al., 2000).

3. Application of the model

The influence of the aggregate composition (number and orientation of grains) on the macroscopic response and the slip heterogeneity is principally studied under different cyclic loadings with strain and stress-controlled situations. The model capability to reproduce the multiaxial ratcheting represents another main objective of this work. Six initially random crystal distributions (40, 200, 300, 400, 504 and 2016 grains, referred to respectively, G-40, G-200, G-300, G-400, G-504 and G-2016) are thus considered. Assumed to be a single-phase FCC type, the Euler angles which define the orientation of each grain within these distributions are numerically generated in a random manner by a small program. Macroscopically, the theoretical initial isotropy of these distributions is almost preserved. For minimizing the calculation time (CPU), the G-200 distribution is practically an optimum compromise as it has been shown in Abdul-Latif et al. (1998). The model parameters (Table 1) have been therefore calibrated (Dingli et al., 2000) with this aggregate using some experimental databases of 316L stainless steel at room temperature (Calloch, 1997). It is important to keep in mind that this calibration process has been achieved using only those experimental results obtained under strain-controlled condition. In fact, according to Calloch (1997), two cyclic tests under strain-controlled condition have been conducted utilizing thin-walled tubes: tension–compression (TC), and out-of-phase tension–torsion, with a sinusoidal waveform and a phase lag of 90° between the two sinusoidal signals (TT90). In each case, the maximum von-Mises equivalent strain is 0.5% during the test.

Several numerical simulations are performed under stress-controlled condition reproducing the ratcheting behavior of stainless steel 316L using the six aggregates. The same cyclic loading path proposed by Portier et al. (2000) is applied during which the multiaxial ratcheting behavior of polycrystals can be appropriately described. This loading is defined as follows (Fig. 2): Bow-tie (path 1) and reverse bow-tie (path 2) cyclic loading situations of three sequences (phases) with different mean stresses (0, 55 and 0 MPa) are respectively imposed with a constant shear strain amplitude of 1%. Note that whatever the used path and the applied phase, a constant stress amplitude of 34 MPa is imposed. Note that path 1 begins with an increase of the axial stress, while path 2 begins with a decease of the axial stress.

Table 1
Identified model constants of stainless steel 316L

λ (MPa)	μ (MPa)	α	k_0 (MPa)	z	K	Q (MPa)	b	h_1	h_2	h_3	h_4	h_5	h_6
136,400	70,300	3×10^{-8}	39.1	10.4	23	394	23	1	1.31	0.96	1.37	1.3	2.57

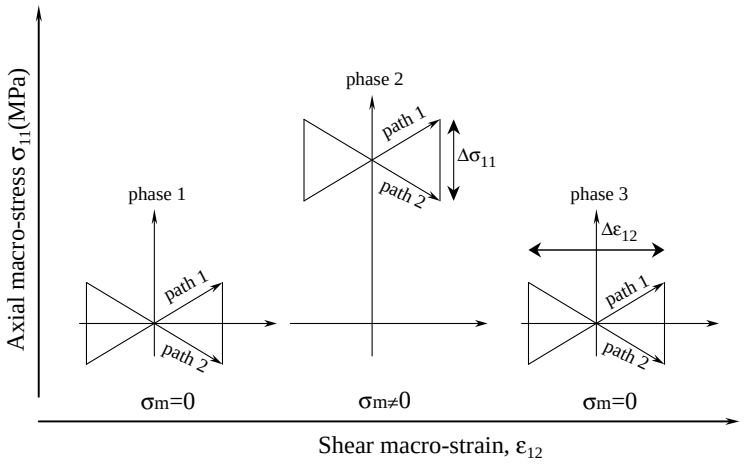

Fig. 2. Bow-tie (path 1) and reverse bow-tie (path 2) multiaxial cyclic loading paths with different mean stresses.

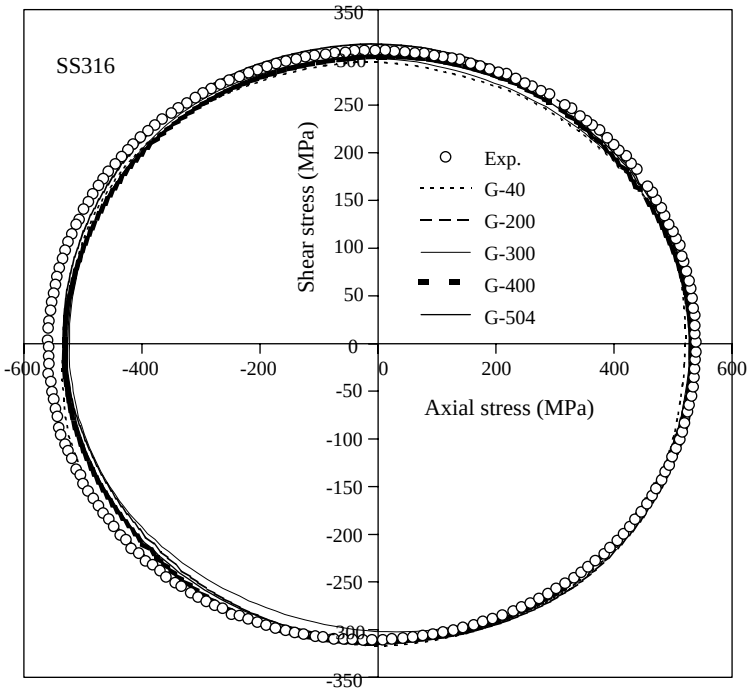

Fig. 3. Comparison between the model and the experiment results for 316L under TT90 (stabilized cycle).

3.1. Predictions under strain-controlled condition

In this paragraph, the overall and local cyclic responses of polycrystals are predicted under strain-controlled loading situation. As an example of cyclic stabilization in TT90, Fig. 3 demonstrates a comparison between the experimental result and predictions of five aggregates (G-40, G-200, G-300, G-400 and

G-504). Obviously, the overall responses of these five aggregates which describe appropriately the cyclic behavior of this alloy, are almost the same.

Under this loading situation, the interpretation of the practically similar overall responses of the five aggregates is based on the aggregate behavior at the lower level, i.e., the granular one. In fact, the axial stress of each grain σ_{11}^{g} is recorded, as an example, at the end of loading and the mean granular stress of each aggregate is then calculated. The five aggregates give almost the same mean granular stress as shown in Fig. 4. This gives an appropriate indication related to the similar overall responses of these aggregates. In order to better understand the model behavior in TT90, the granular axial elastic, inelastic and total strains are recorded (Fig. 5) for each aggregate at the end of loading. This figure highlights the fact that the granular behavior has a heterogeneous nature whatever the aggregate type, reflecting the aptitude of this approach in describing this heterogeneity. At this point, the parameter α (3×10^{-8}) leads to an instantaneous elastic effect and viscoplastic relaxation at the steady state (Abdul-Latif et al., 2002). If these two conditions are well respected, the overall cyclic kinematic and isotropic hardenings will be successfully described. Hence, at the cyclic steady state, the term $\alpha(\underline{s}^{g} - \underline{S})$ gives a certain equilibrium between the first two terms in the left hand side of Eq. (20) leading therefore to relatively smooth interactions between grains and their matrix. The heterogeneity of the granular elastic behavior (Fig. 5a) dictated by the interaction law, induces naturally the global kinematic hardening effect (Dingli et al., 2000; Abdul-Latif et al., 2002). This can be interpreted by the fact that the intergranular accommodation has an elastic nature (Rougier et al., 1994). Fig. 5b illustrates in a clear manner the granular heterogeneous viscoplasticity at the steady state in function of all the employed aggregates. This heterogeneity remains obvious even in the case of total granular strain where the strain fluctuation is around 0.005 (Fig. 5c). The mean values of these heterogeneous responses at the granular level of the aggregates (stress and elastic, viscoplastic and total strains) are almost similar leading consequently to practically the same predictions whatever the aggregate type.

At the css level, it is noticed that the aggregate type has a primordial role on the heterogeneity of the accumulated slip as demonstrated in Fig. 6. In order to correctly understand this figure, the final projected accumulated slip (γ_{ac}) should be clearly defined. Its determination is performed at the end of loading by a projection process of all plastified slip systems in the aggregate of grains with respect to the applied loading direction. For further details about this process, the reader is to refer to Abdul-Latif et al. (1999). An

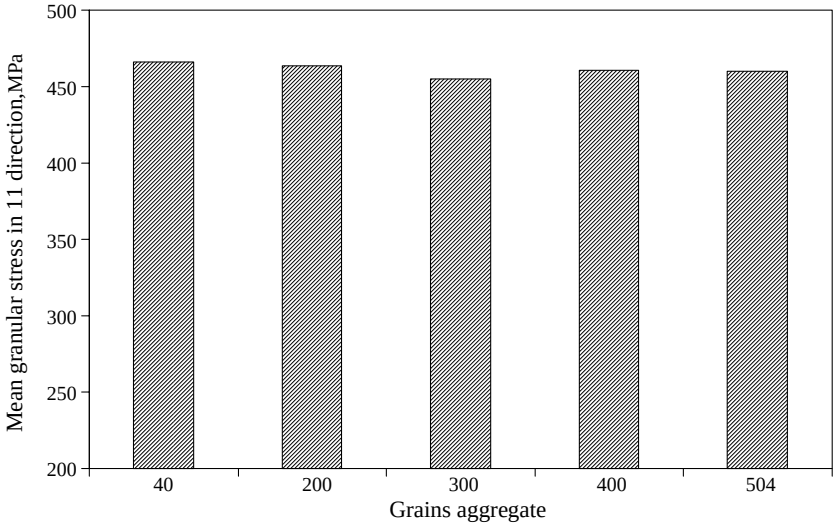

Fig. 4. Effect of the aggregate of grains type on granular stress in TT90 (at the end of loading).

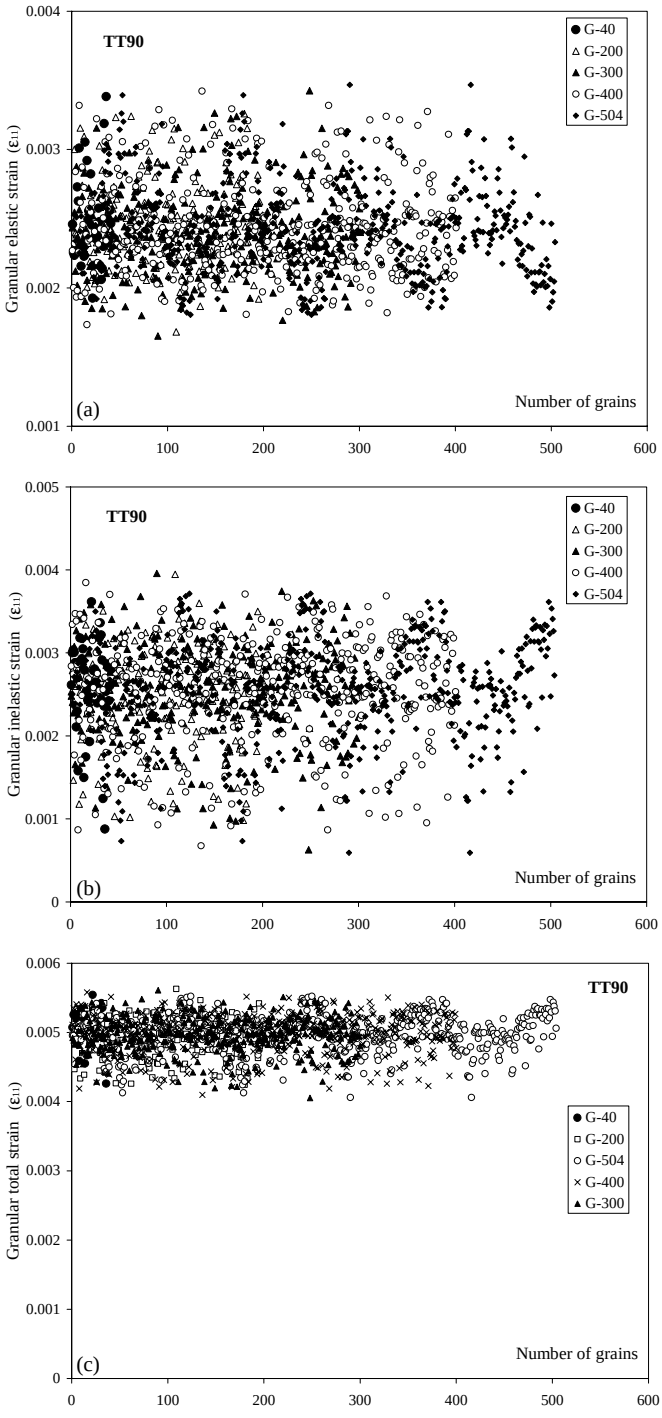

Fig. 5. Axial granular strains evolution: (a) elastic, (b) inelastic and (c) total under TT90 cyclic loading path for different aggregates.

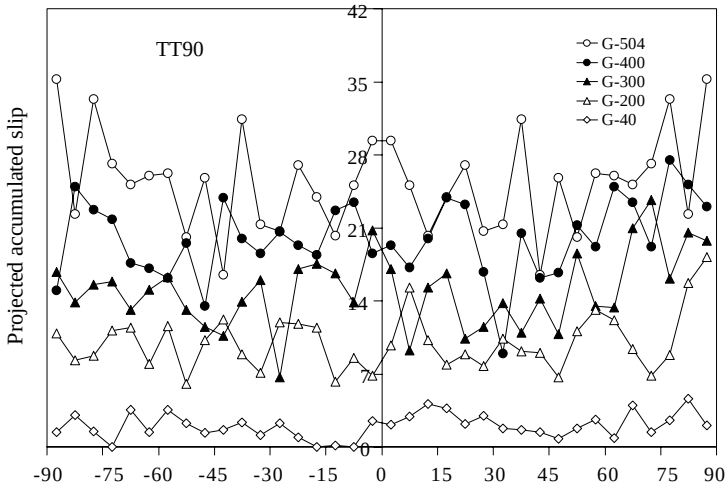

Fig. 6. Projected accumulated slip distribution with respect to the applied load (TT90) using different aggregates.

examination of Fig. 6 shows the non-symmetrical projected accumulated slip distribution with respect to the loading axis for each aggregate (except for the G-504). It is clear that when the number of grains in the aggregate is increased, the number of plastified systems increases leading consequently to a noticeable change in the slip distribution fashion. As a result, a highest value is thus recorded in the case of the G-504. Moreover, it is also observed that for TT90, two relatively maximum values are generally recorded in around 0° and in ±90° directions.

3.2. Predictions under stress-controlled condition

Another main objective of this study is to predict the polycrystal cyclic behavior under stress-controlled conditions, notably the multiaxial ratcheting phenomenon. In general, the later is captured in the case where the mean stress is different to zero. Several numerical simulations are conducted reproducing the multiaxial ratcheting behavior of stainless steel 316 using the six aggregates. As shown above, these distributions give almost the same overall responses under strain-controlled condition. Whereas, under the stress-controlled condition, each aggregate behaves differently even when the applied mean stress is equal to zero. Hence, the effect of the aggregate type on the mechanical response is studied using the bow-tie cyclic loading path (Fig. 2). The two paths (1 and 2) are used and all the above aggregates are numerically tested. Qualitatively, Fig. 7 displays (for path 1) the model ability to describe correctly the ratcheting phenomenon whatever the aggregate type. In fact, during the first phase of 30 cycles (a zero mean stress), a small positive ratcheting of the axial strain is reproduced up to the cyclic stabilization. A non-zero mean stress of 55 MPa is then imposed in the second phase. A noticeable ratcheting behavior of the overall axial strain is fairly well described by the model. A partial recovery is recorded during the third phase (a zero mean stress). Moreover, this figure shows the fact that the aggregate type has a significant influence on the overall response. In other words, the differences increase, in general, as the number of grains in the aggregate almost decreases. In addition, as the number of grains increases, the overall response converges generally, i.e., the aggregates G-300, G-400, G-504 and G-2016 have practically an equivalent response. However, the interpretation of the small differences recorded in their responses is not yet clear at least in this work. This result points obviously out a considerable sensitivity of the model to this factor. Hence, one can consider that this factor represents henceforth a model parameter needing identification.

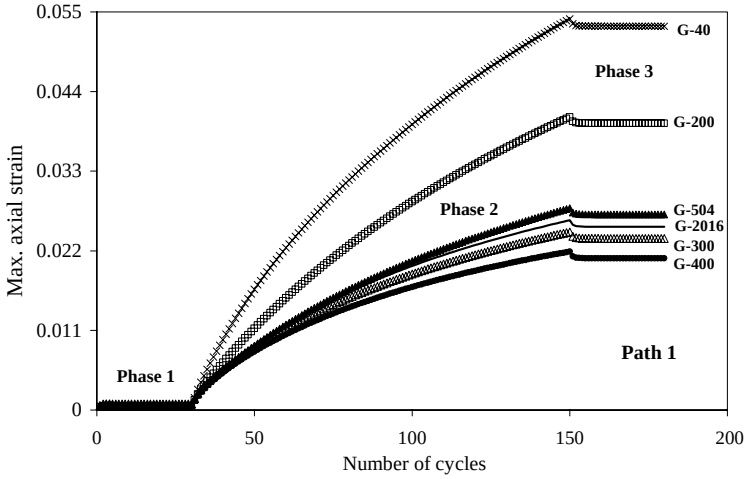

Fig. 7. Effect of the grains aggregate type on the overall predicted responses during the three phases of bow-tie cyclic loading (path 1).

The mean granular axial strain is predicted for each aggregate at the end of the second phase of applied loading (path 1) where the maximum divergence is recorded. Contrary to the granular response under strain-controlled condition, Fig. 8 shows a remarkable variation of such a strain with respect to the aggregate type. Based on this results, one can interpret the change of the overall multiaxial ratcheting response by the change of the aggregate type. This response is principally dictated by the interaction law (Eq. (20)). Indeed, the parameter α has been determined in such a manner that the instantaneous elastic effect and the viscoplastic relaxation are ensured. So that, the overall cyclic kinematic and isotropic hardenings are successfully described. It is well-known that the ratcheting behavior is mainly governed by the kinematic hardening. Hence, with $\alpha = 3 \times 10^{-8}$, the interaction law leads to a heterogeneous granular elastic behavior (Fig. 9a) and consequently to a natural description of the global kinematics hardening. This gives consequently a reasonable description of the ratcheting behavior of polycrystals. The instantaneous

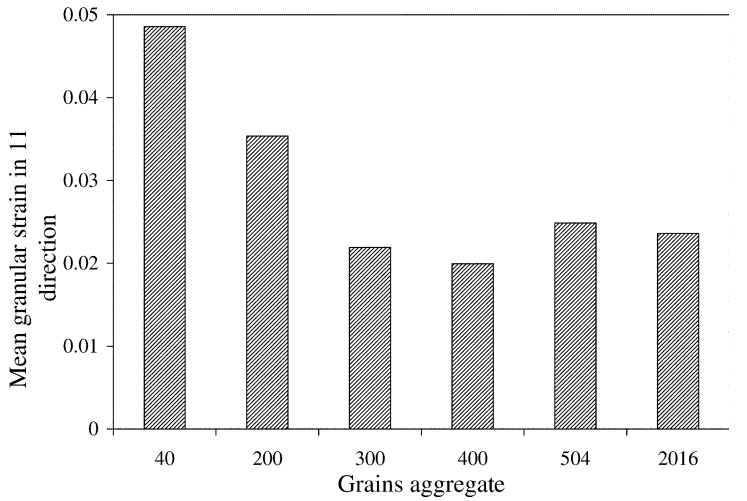

Fig. 8. Effect of the aggregate type on granular strain under bow-tie cyclic loading path (at the end of path 1).

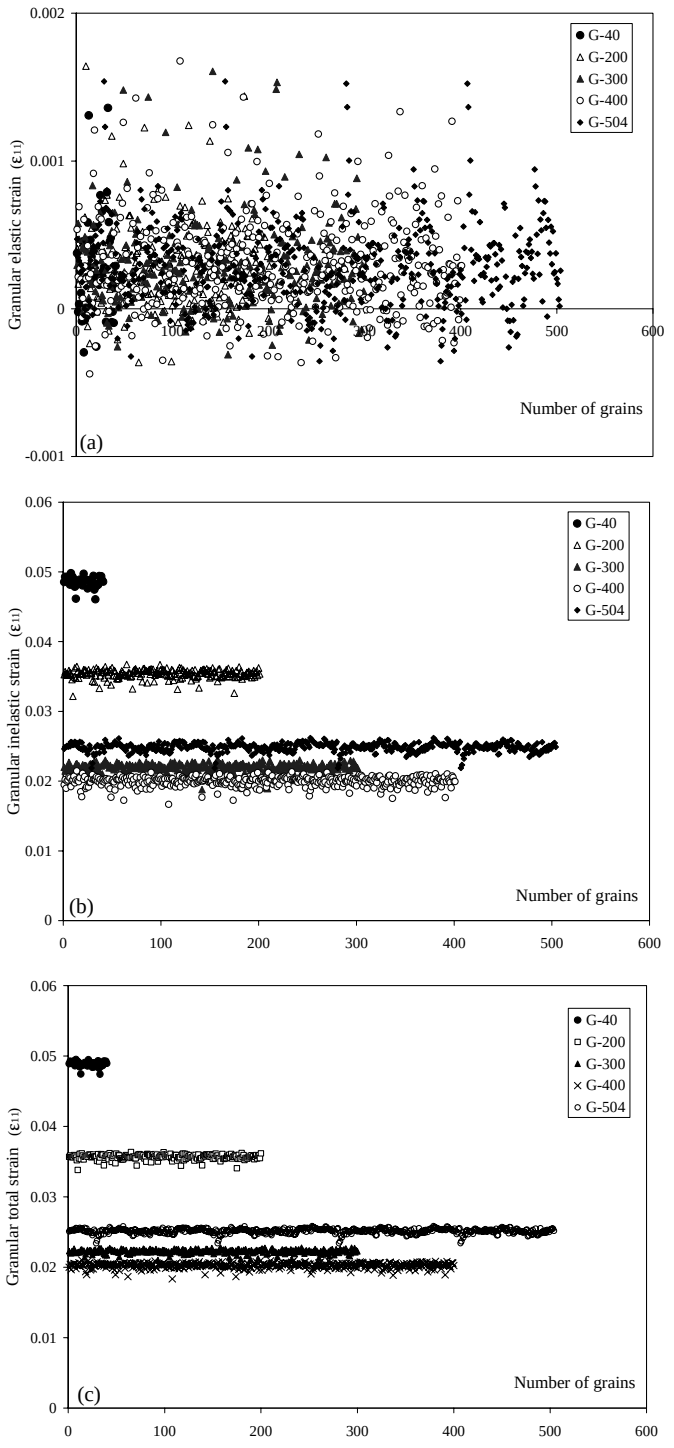

Fig. 9. Axial granular strains evolution: (a) elastic, (b) inelastic and (c) total under bow-tie cyclic loading path for different aggregates.

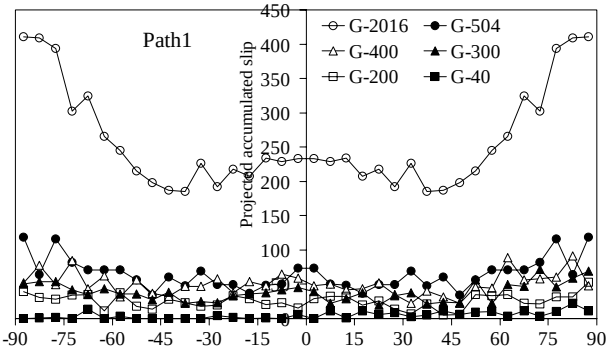

Fig. 10. Projected accumulated slip distribution with respect to the applied loading (path 1).

granular elastic effect gives a progressive decreasing of the activated slip systems. The granular viscoplastic relaxation at the end of the second phase for each aggregate is almost homogenous (Fig. 9b). It is obvious from this figure that the inelastic granular behavior of each aggregate is different in comparison with the other aggregates. For example, the G-40 has the most important axial inelastic granular strain value (about 0.05), while the lowest value (around 0.02) is recorded for the G-400. For this reason, the overall response of this aggregate has the highest value concerning the multiaxial ratcheting during path 1. It is worth emphasizing that, for a given α, the elastic and inelastic strain behaviors of each grain are also sensitive to the model parameters and the type of the used aggregate (Dingli et al., 2000).

Let us show now the local predicted heterogeneity relative to this loading situation. An examination of Fig. 10 reveals, as given above, that the local heterogeneity (γ_{ac}) changes with the change of the aggregate type for a given loading condition, i.e., a higher value of the (γ_{ac}) is recorded for a higher number of grains. Moreover, the (γ_{ac}) is symmetric only in the G-504 and the G-2016 cases and becomes more important in $\pm 90°$ and less important in $\pm 45°$ directions.

A quantitative comparison between the model prediction and experimental results of multiaxial ratcheting is presented in Fig. 11 for 316L stainless steel. This figure characterizes the overall axial strain

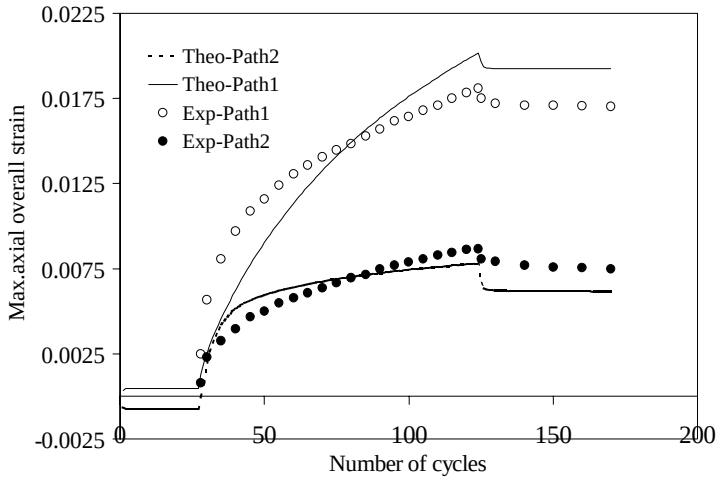

Fig. 11. Comparison between the overall predicted response and the experiment result during the three phases of bow-tie and reverse bow-tie cyclic loadings using the G-400.

evolution versus the number of cycles. The multiaxial ratcheting behavior presented is induced by the bow-tie (path 1) and reverse bow-tie (path 2) at different mean stresses (0, 55 and 0 MPa). Since the 400-grain aggregate gives relatively the best prediction (among the six) in comparison with the material ratcheting behavior, thus the numerical simulation in this figure are performed with this aggregate. The polycrystal behavior during path 1 was already described above. As far as the ratcheting behavior under path 2 is concerned, the related prediction is characterized by a small negative ratcheting of the overall axial strain reproducing satisfactorily the real material behavior in the first phase. A remarkable overall ratcheting of

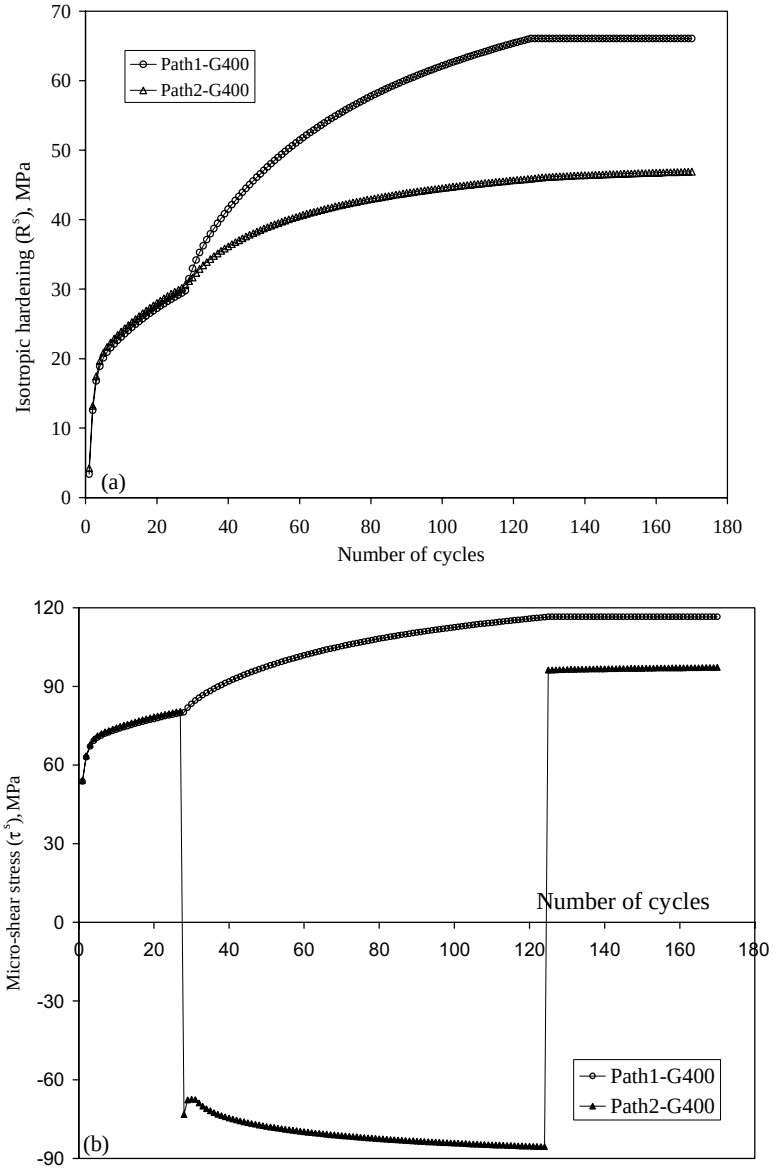

Fig. 12. Predicted evolution of the (a) intragranular isotropic hardening and (b) resolved shear stress, for a given activated slip system during the three phases of bow-tie and reverse bow-tie cyclic loadings.

the axial strain evolution is observed in the second phase. Note that the stainless steel behavior shows that this ratcheting is almost faster and more important for path 1 due to the change of the applied loading nature. Again, the model demonstrates an appropriate capability for describing such a behavior. Finally, as in path 1, a partial recovery is experimentally observed up to the cyclic steady state condition. Here also, the model describes correctly this recovery in path 1 as well as in path 2. It is important to note that we did not use any experimental cyclic result of stress-controlled condition during the identification process of the model parameters. In order to show how the model can appropriately reproduce the polycrystal cyclic behavior during paths 1 and 2, the intragranular isotropic hardening (R^s) and shear stress (τ^s) evolutions are studied. Fig. 12a and b describes R^s and τ^s evolution respectively versus the number of cycles for a given activated slip system in a well-plastically deformed given grain among 400 grains. The first remark is related to the fact that the evolution of these variables is somewhat similar during the first phase of applied paths. Whereas, a relative strong change takes place at the beginning of the second phase (mean stress = 55 MPa). More clearly, the intragranular isotropic hardening becomes more important for path 1. This is mainly induced by the evolution of the activated slips as given in Fig. 13, in which their rates of change remain more or less slow for path 1, while, a sudden decreasing is recorded in path 2. Accordingly, an abrupt change of τ^s is observed as soon as the second phase of path 2 begins. Then, another steeply increase of τ^s takes place during this loading when the third phase is applied. With this rapid change of the mean stress (from 55 to 0 MPa), a sudden increase in activated slip systems occurs for path 2 and stabilizes then rapidly. The same statement is observed for path 1, but an abrupt decrease of activated slip systems is recorded, which gives an interpretation of R^s and τ^s evolutions (steady state) during this phase. Moreover, in path 2, these variables continue their positive evolutions due to the increase of activated slip systems (Fig. 13).

Another example of classical multiaxial tension–torsion ratcheting at 25 °C studied experimentally by Portier et al. (2000) is simulated here by the model using the 400-grain aggregate. In fact, five sequences of cyclic total shear strain amplitudes ($\Delta\varepsilon_{11}$: 0.1% (100 cycles), 0.2% (95 cycles), 0.35% (55 cycles), 0.5% (45 cycles) and 0.75% (65 cycles)) are imposed during which a constant primary axial stress σ_{11} of 100 MPa is applied. Fig. 14 shows a comparison between prediction and the experimental maximum axial strain evolution versus number of cycles. This figure reveals obviously that the model can successfully describe the axial strain ratcheting response of stainless steel 316L.

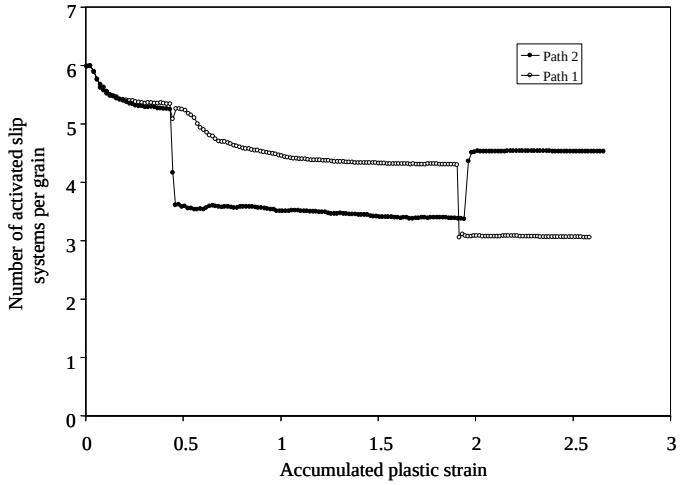

Fig. 13. Variation of the average predicted activated slip systems within the aggregate of the 400 grain during the three phases of bow-tie and reverse bow-tie cyclic loadings.

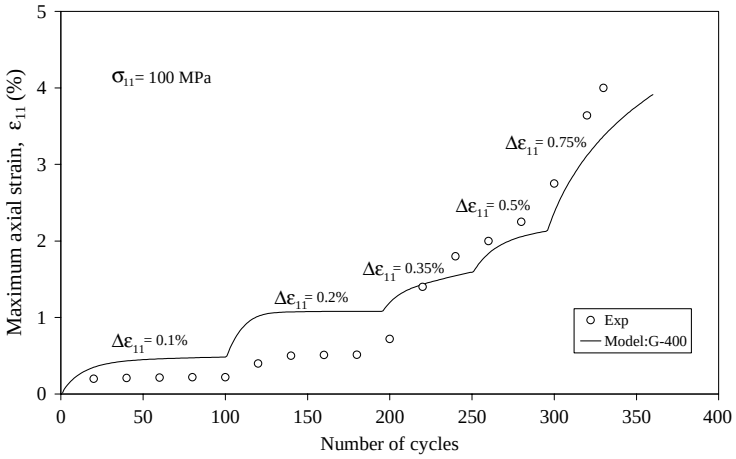

Fig. 14. Comparison between the overall predicted response and the experiment result of the maximum axial strain evolution during the cyclic loading using the G-400.

4. Conclusion

The faithful description of many cyclic phenomena such as Bauschinger effect, strain memory effect and additional hardening has been already demonstrated by the model (Dingli et al., 2000; Abdul-Latif et al., 2002) under strain-controlled conditions.

The model highlights the fact that the heterogeneous of the granular behavior is appropriately described and is strongly influenced by the aggregate type and the applied loading path. Since the model reproduces naturally the global kinematic hardening (due to the granular elastic heterogeneity), therefore the ratcheting behavior can be successfully described.

The effect of the aggregate of grains type (i.e., the number and the orientation of grains) on the nonlinear strain–stress polycrystals behavior is qualitatively investigated using six different aggregates. Several numerical simulations point out the fact that the aggregate type has a fundamental influence on the predicted overall response under cyclic stress-controlled loading, while under strain-controlled situation, this parameter has practically a negligible effect. Hence, one can conclude that the aggregate of grains represents a parameter of the model needing identification.

Comparisons between the experimental result of stainless steel 316L and the model prediction reveal its capability to appropriately reproduce the multiaxial ratcheting behavior of this alloy (despite the high complexity of such a behavior) and its sensitivity to the aggregate composition (number and orientation of grains).

References

Abdul-Latif, A., Saanouni, K., 1997. Effect of some parameters on the plastic fatigue behavior with micromechanical approach. Int. J. Damage Mech. 6, 433.

Abdul-Latif, A., Dingli, J.Ph., Saanouni, K., 1998. Modeling of complex cyclic inelasticity in heterogeneous polycrystalline microstructure. J. Mech. Mater. 30, 287.

Abdul-Latif, A., Ferney, V., Saanouni, K., 1999. Fatigue damage of waspaloy under complex loading. ASME J. Eng. Mat. Tech. 121, 278.

Abdul-Latif, A., Dingli, J.Ph., Saanouni, K., 2002. Elasto-inelastic self-consistent model for polycrystals. J. Appl. Mech. 69, 309.

Bennett, V.P., McDowell, D.L., 2003. Polycrystal orientation distribution effects on microslip in high cycle fatigue. Int. J. Fatigue 25, 27.

Budiansky, B., Wu, T.T., 1962. Theoretical prediction of plastic strains of polycrystals. In: Proc. 4th US Nat. Cong. Appl. Mech. ASME, p. 1175.

Cailletaud, G., 1987. Une Approche Micromécanique Phénoménologique du Comportement Inélastique des Métaux. Thèse d'état, Université Paris VI.

Calloch, S., 1997. Essais Triaxiaux Non-proportionnels et Ingénierie des Modèles de Plasticité Cyclique. Thèse de Doctorat, Université Paris 6.

Dingli, J.P., Abdul-Latif, A., Saanouni, K., 2000. Predictions of the complex cyclic behavior of polycrystals using a new self-consistent modeling. Int. J. Plasticity 16, 411.

Dvorak, G.J., Benveniste, Y., 1996. On micromechanics of inelastic and piezoelectric composites. In: Tatsumi, T., Watanabe, E., Kambe, T. (Eds.), ICTAM. North-Holland, p. 217.

François, D., Pineau, A., Zaoui, A., 1993. Comportement Mécanique des Matériaux. Hermes, Paris.

Kröner, E., 1961. Zur Plastichen Verformung des Vielkristalls. Acta. Metall. 9, 155.

Molinari, A., Canova, G.R., Ahzi, S., 1987. A self-consistent approach of the large deformation viscoplasticity. Acta. Metall. 35, 2983.

Molinari, A., Ahzi, S., Kouddane, R., 1997. On the self-consistent modeling of elasto-plastic behavior of polycrystals. Mech. Mater. 26, 43.

Pilvin, P., 1990. Approches Multiéchelles pour la Prévision du Comportement Anélastique des Métaux. Thèse de Doctorat, Université Paris 6.

Portier, L., Calloch, S., Marquis, D., Geyer, P., 2000. Ratchetting under tension–torsion loading: experiments and modelling. Int. J. Plasticity 16, 303.

Rougier, Y., Stola, C., Zaoui, A., 1994. Self-consistent modeling of elastic–viscoplastic polycrystals. C.R. Acad. Sci., Paris 319, 145.